

# LOW-MOTIONAL-IMPEDANCE HIGHLY-TUNABLE I<sup>2</sup> RESONATORS FOR TEMPERATURE-COMPENSATED REFERENCE OSCILLATORS

Gavin K. Ho, Krishnakumar Sundaresan, Siavash Pourkamali, Farrokh Ayazi  
Georgia Institute of Technology, Atlanta, Georgia, USA

## ABSTRACT

A new capacitive micromechanical resonator design optimized for high  $Q$ , low motional impedance, and large tuning range is presented. The I<sup>2</sup> resonator was fabricated using a conservative, by present standards, HARPSS-on-SOI process, and demonstrated quality factors up to 57000 in vacuum. From the designed resonators between 3MHz and 6MHz, the lowest measured impedance is 2.4k $\Omega$  and the largest electrostatic tuning coefficient is -10ppm/V<sup>2</sup>. An oscillator interface circuit comprising of a trans-impedance amplifier and an automatic tunable charge pump providing an automatic temperature-compensating bias voltage was also designed and fabricated in a standard 0.5 $\mu$ m CMOS process. Preliminary tests show temperature drift reduction of a 4MHz resonator from 2400ppm to 240ppm over a 90°C range.

## 1. INTRODUCTION

Frequency references are required in all clocked electronic systems, including communication circuits, microprocessors and sampled signal processing circuits. Typical quartz-based oscillators suitable for these applications have quality factors in excess of 10000 and temperature variation in the range of 50ppm over 100°C [1]. These, however, cannot be integrated in the same package with the electronics, thus increasing the size and cost of the system.

Reference oscillators have stringent requirements on temperature stability and phase noise. These requirements translate into resonator requirements of frequency tunability for temperature compensation and high quality factor. Low motional impedance also is desirable to minimize the power consumption. For optimal performance, the interface circuit should include an amplifier circuit that minimizes  $Q$  loading, and a means to compensate for the frequency-temperature drift of the resonator.

The latest MEMS-based oscillator technology includes a 60MHz wine-glass mode resonator [2] and a 12MHz square lamè mode resonator [3]. These, as well as other resonator geometries, each have their unique features, but do not meet all the above requirements. HF and VHF beam resonators have high tunability, but typically have low  $Q$  [4]. Bulk mode disk [2,5] and extensional-mode resonators [6] have high  $Q$ , but suffer from poor tunability. In this work, we present a new resonator design optimized for high  $Q$ , low motional impedance, and high electrical tunability. When interfaced with a standard CMOS IC with an amplifier and a temperature-sensitive resonator biasing circuitry, these features enable a low power consumption oscillator with improved frequency stability.

## 2. I<sup>2</sup> RESONATOR DESIGN

From the electromechanical model for a symmetrical two-port capacitive resonator, the motional resistance

$$R_m = \frac{k_n}{\omega_n Q \left( V_p \frac{dC}{dx} \right)^2} = \frac{k_n d^4}{\omega_n Q A_e^2 V_p^2 \epsilon^2} \quad (1)$$

is inversely proportional to the square of the polarization voltage  $V_p$  and electrode overlap area  $A_e$ , and is also dependent on the capacitive gap size  $d$  to the fourth power. The amount of electrostatic frequency tuning

$$\frac{\Delta f}{f_0} = \frac{\epsilon A_e}{k_n d^3} V_p^2 \quad (2)$$

is linearly dependent on  $V_p^2$ ,  $A_e$ , and  $d^3$ . The most common approaches to reduce  $R_m$  and increase  $\Delta f/f_0$  involve decreasing  $d$  or increasing  $V_p$  [7]. Although these techniques are quite effective, they pose stringent fabrication demands and require large voltages. In this work, the low  $R_m$  and high tuning coefficient  $\Delta f/(f_0 V_p^2)$  are achieved by increasing the capacitive transduction area  $A_e$  while maintaining a small resonator effective stiffness  $k_n$ . In an extensional-mode resonator, this can be implemented by extending electrode length  $L_e$ , and using a small rod to provide stiffness (Fig. 1). This design resembles the letter “I”, which we call an I-BAR (bulk acoustic resonator). This concept was extended further by placing two “I” sections adjacent to each other to form the I<sup>2</sup> resonator (Fig. 2).

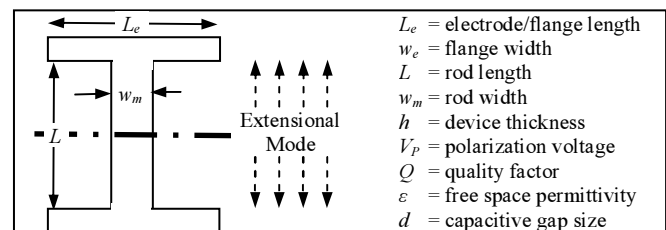


Figure 1: I-BAR resonator design concept for low motional impedance and high tunability

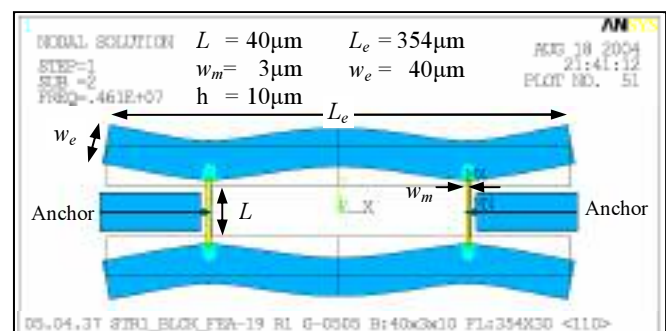


Figure 2: ANSYS modal analysis of a 4.6MHz I<sup>2</sup>-resonator

### 3. FABRICATION & EXPERIMENTAL DATA

Fig. 3 shows an SEM of a 10 $\mu\text{m}$ -thick single crystal silicon HARPSS-on-SOI [5] 4MHz  $I^2$  resonator with 270nm gaps. The entire resonator body and two anchors are made of single crystal silicon (SCS) with a resistivity of 0.01-0.02 $\Omega\text{cm}$ . LPCVD trench-refilled doped polysilicon electrodes are connected to a polysilicon pad that is directly on the SCS. The vertical capacitive gap is defined by a layer of sacrificial LPCVD oxide deposited prior to the polysilicon trench-refill process.

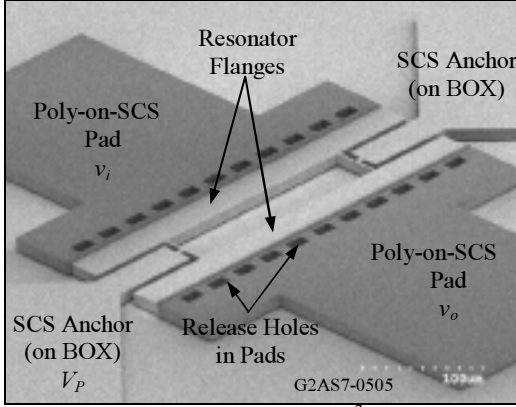


Figure 3: SEM of a 10 $\mu\text{m}$  thick SCS  $I^2$  resonator (designed in Fig. 2) fabricated using the HARPSS-on-SOI process with 270nm gaps

Since low device impedance and tunability are the main objectives, device frequencies only up to 6MHz were designed. The highest  $Q$  measured from all the designs was approximately 57000 at 3.94MHz (Fig. 4) from the device in Fig. 3. Table 1 summarizes the specifications of several  $I^2$  resonators.

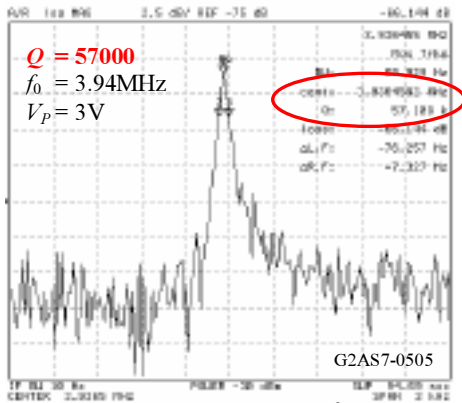


Figure 4: Frequency response of the  $I^2$  resonator with the highest  $Q$  measured (from device in Fig. 3 with  $V_p=3\text{V}$ ).

### Motional Impedance

The open-loop frequency response of the resonators was measured using an HP4395A network analyzer directly without any signal conditioning. All data reported were collected in high vacuum from wire-bonded samples, except for the temperature characterization data. The device impedance can be extracted from the insertion loss using:

$$R_{MEAS} = 50 \left( 10^{\frac{IL_{dB}}{20}} - 1 \right) \quad (3)$$

The lowest impedance measured is 2.4k $\Omega$  from a 5.53MHz resonator with  $V_p=55\text{V}$  (Fig. 5). The impedances of several resonators are plotted versus  $1/V_p^2$  in Fig. 6. These plots are linear, as expected from (1), but exhibit a constant offset of 1k $\Omega$  to 5k $\Omega$ .

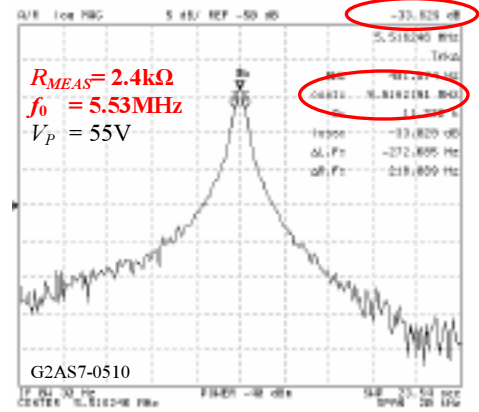


Figure 5: Frequency response of the lowest impedance and highest frequency HARPSS  $I^2$  resonator

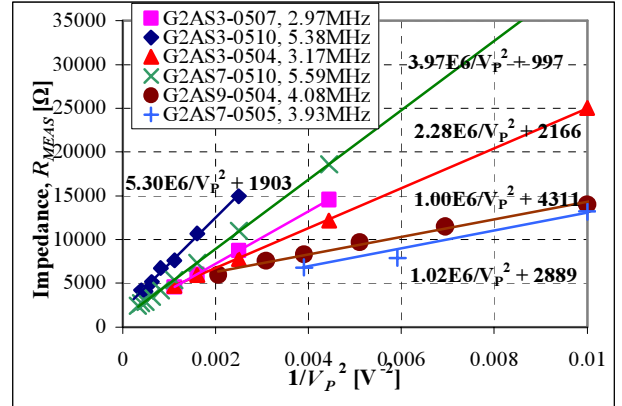


Figure 6: Measured impedance vs. inverse square of the polarization voltage for the  $I^2$  resonators, showing a linear trend with a constant loading ( $R_s$ ) for each data set

Table 1: Experimental Data Highlights

Device ID	Geometry			Measurement							Features	
	$L \times w_m \times h$ [ $\mu\text{m}$ ]	$L_e \times w_e$ [ $\mu\text{m}$ ]	Etch Holes?	$f_{\text{test, nom.}}$ [MHz]	$V_{P,MAX}$ [V]	$IL@V_{P,MAX}$ [dB]	$Q_U$	$Q_L$	$R_{MEAS}$ [ $\Omega$ ]	$R_s$ [ $\Omega$ ]		Tuning Coefficient
G2AS3-0507	60 $\times$ 5 $\times$ 10	497 $\times$ 40	Yes	2.97	30	39.347	12849	9274	4588	1218	-10ppm/V <sup>2</sup>	Most Tunable
G2AS7-0510	40 $\times$ 5 $\times$ 10	279 $\times$ 30	Yes	5.59	55	33.829	23167	11222	2409	997	-4ppm/V <sup>2</sup>	Highest $f_i$ , Lowest $R_m$
G2AS9-0504	40 $\times$ 3 $\times$ 10	354 $\times$ 30	Yes	4.08	22+	41.600	35497	20441	5961	4311	-7.5ppm/V <sup>2</sup>	Interfaced Oscillator
G2AS7-0505	40 $\times$ 3 $\times$ 10	354 $\times$ 30	No	3.93	16+	42.758	57109	30495	6812	2889	-6ppm/V <sup>2</sup>	Highest $Q$

These offsets are identified as resistances  $R_S$  in series with the input and output of the resonator. An  $R_S$  of 997 $\Omega$  was extracted for the nominally 5.59 MHz resonators in Fig. 5. Removing this series resistance from the measured impedance of 2.4k $\Omega$  yields a motional impedance of 1.4k $\Omega$ !

The extracted  $R_S$  can be attributed to various resistances from the  $V_P$  source node to the device input and output nodes. Although there is no metallization, contact resistances between the doped-polysilicon pads and Al-Si bonding wires were measured to be no more than 5 $\Omega$ . In two-port extensional-mode resonators, the input and output electrode capacitive displacements are in phase, and the generated current must be provided from the  $V_P$  source pad. Thus, any impedance in this path, including the resistance of the resonator body, would also load the resonator. In addition, the resistance of the trench-refilled polysilicon electrodes may also be a source of loading.

### Quality Factor Variation

Quality factor variation between various resonators was observed (Table 1); lower  $Q$ s were measured from resonators with etch holes in the flanges (Fig. 7). These etch holes were placed to reduce the mass loading and release-etch time. The  $Q$  reduction from these features is unexpected, and we speculate that it is caused by mode shape distortion. This however is not of great concern, since solid devices have been reliably fabricated (Fig. 3).

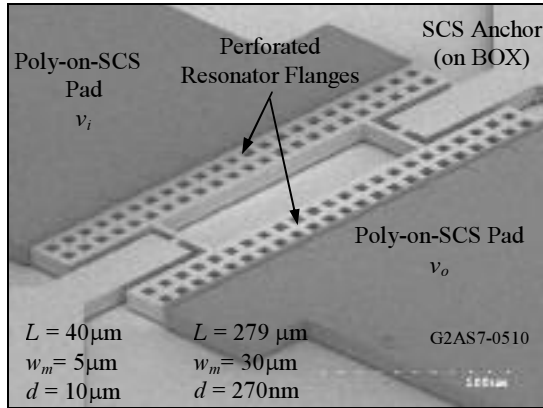


Figure 7: SEM of an  $I^2$  with etch-holes in the flanges which demonstrated a lower quality factor (see Fig. 4 and Table 1) than  $I^2$ s with solid-flanges

The quality factor of the resonators was also observed to decrease with increasing  $V_P$  (Fig. 8). Although this was not the first observation of this phenomenon, it was the most severe case of  $Q$  degradation measured. At large  $V_P$ , we were very cautious to avoid saturation, and therefore this  $Q$  decrease was not caused by nonlinearities.

Earlier, we identified some additional series impedance  $R_S$  from the  $R_{MEAS}$  vs  $V_P^{-2}$  plots in Fig. 6. Since the motional impedance of the resonators is high at low  $V_P$ , the effect of loading from these  $R_S$  is minimal. However, at larger  $V_P$ , the values of  $R_m$  and  $R_S$  are comparable, and electrical loading will reduce the  $Q$ . Recalling the expressions for the loaded and unloaded quality factor,  $Q_L$  and  $Q_U$ , respectively, of a series RLC:

$$Q_L = \frac{\omega L_m}{R_{MEAS}}, Q_U = \frac{\omega L_m}{R_m} \quad (4),(5)$$

the  $Q_L$  can then be found from  $Q_U$ ,  $R_m$ , and  $R_S$ :

$$Q_L = Q_U \frac{R_m}{R_{MEAS}} = Q_U \frac{R_m}{R_m + R_S} \quad (6)$$

Taking  $Q_U$  as the quality factor measured at low  $V_P$ ,  $R_S$  from Fig. 6, and  $R_m = R_{MEAS} - R_S$ , the estimated loaded  $Q$  from (6) is also plotted in Fig. 8. The experimental data and the estimated  $Q_L$  correlate quite well, providing sufficient evidence that the reduction in  $Q$  is caused by electrical loading and confirms the value of  $R_S$  in the signal path.

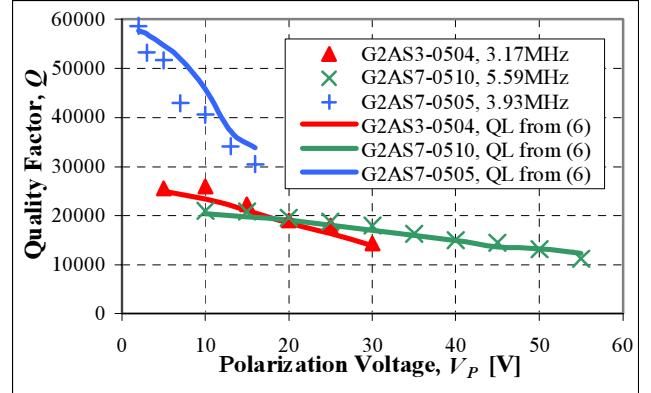


Figure 8: Measured resonator loaded quality factor and estimated loaded  $Q$  variation with polarization voltage

### Electrostatic Tuning

The normalized frequency shift due to electrostatic tuning is plotted in Fig. 9 for several resonators. Electrostatic tuning coefficients (ETC) as large as -10ppm/ $V^2$  were measured in the 3MHz resonators. Over 9000ppm frequency shift was measured for a polarization voltage change from 5V to 30V. In higher frequency resonators, reduction of the tunability is expected. At 5.6MHz, the tuning coefficients were measured to be -4ppm/ $V^2$ , and a frequency shift of 10000ppm was measured for polarization voltage change of 5V to 50V. These large electrostatic tuning coefficients make electrostatic frequency tuning a suitable option for compensation of frequency-temperature drift.

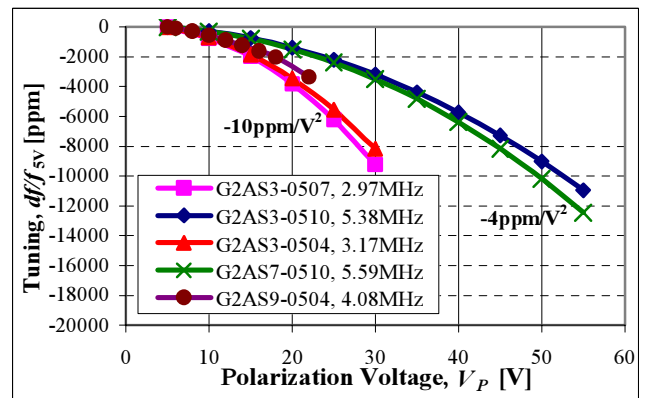


Figure 9: Normalized electrostatic frequency tuning for various designs of the  $I^2$  resonator

## Design Validation

The effective resonator stiffness parameter  $k_n$  is contained in both equations (1) and (2), but since the geometry and mode shape of the  $I^2$  are complex, evaluation of  $k_n$  by analytical means may not be feasible. Nonetheless, experimental data is available, so the stiffness can be extracted and the gap size can be verified using the two equations (Table 2).

Table 2. Extracted mechanical parameters and gap sizes

Device ID	Frequency $f_0$ [MHz]	Stiffness $k_n$ [N/m]	Effective Mass $m_n$ [kg]	Gap Size $d$ [nm]
■ G2AS3-0507	2.97	$110 \times 10^3$	$320 \times 10^{-12}$	340
◆ G2AS3-0510	5.38	$170 \times 10^3$	$150 \times 10^{-12}$	340
▲ G2AS3-0504	3.17	$88 \times 10^3$	$220 \times 10^{-12}$	340
× G2AS7-0510	5.59	$320 \times 10^3$	$260 \times 10^{-12}$	270
● G2AS9-0504	4.08	$270 \times 10^3$	$410 \times 10^{-12}$	250
+ G2AS7-0505	3.93	$260 \times 10^3$	$430 \times 10^{-12}$	270

The extracted  $k_n$  from the 3.93MHz  $I^2$  resonator (Fig. 3) is used in comparing its performance with a 4MHz clamped-clamped  $80\mu\text{m} \times 3\mu\text{m}$  beam and a 4MHz 940 $\mu\text{m} \times 200\mu\text{m}$  extensional mode resonator (Table 3). Of the three designs, the  $I^2$  has the lowest impedance, a large tuning coefficient, and sufficiently high  $Q$ . These features make the  $I^2$  the most appealing for a temperature-compensated reference oscillator.

Table 3. Comparison of 4MHz resonators

	$I^2+$	CC Beam	Extensional
Dimensions, $L \times w$ [ $\mu\text{m}$ ]	See Fig. 2	80 $\times$ 3	940 $\times$ 200
Device Thickness, $h$ [ $\mu\text{m}$ ]	10	10	10
Electrode Length, $L_e$ [ $\mu\text{m}$ ]	354	80	940
Eff. Stiffness, $k_{\text{eff}}$ [N/m]	$260 \times 10^3$	$5.5 \times 10^3$	$1400 \times 10^3$
Effective Mass, $m_{\text{eff}}$ [kg]	$430 \times 10^{-12}$	$8.7 \times 10^{-12}$	$2200 \times 10^{-12}$
Assumed $Q$	50000	10000	<b>100000</b>
$V_p=5\text{V}$	Impedance [ $\Omega$ ]	<b>860</b>	1700
$d=50\text{nm}$	Tuning, ppm/ $V^2$	-120	-1300
$V_p=10\text{V}$	Impedance [ $\Omega$ ]	<b>3400</b>	7000
$d=100\text{nm}$	Tuning, ppm/ $V^2$	-15	-160

## 4. OSCILLATOR DESIGN & IMPLEMENTATION

The block diagram of the oscillator is shown in Fig. 10. It comprises primarily of a trans-impedance amplifier and an inverting buffer to satisfy the oscillation gain and phase-shift criteria and an on-chip temperature-compensating high-voltage bias generator. The trans-impedance gain of the amplifier is set by a voltage-controlled MOS resistor to prevent resonator saturation.

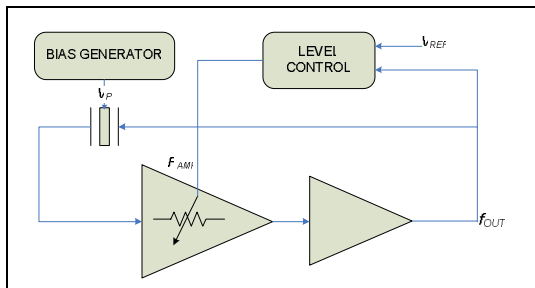


Figure 10: Block diagram of tunable oscillator

To compensate for temperature drift, a varying bias voltage  $V_p$  is used. This voltage is generated on-chip using a charge pump and temperature slope generator. A large voltage in the range of 25V is first generated using a 6-stage Dickson charge pump [8] shown in Fig. 11a. The clocks required for the charge pump are also generated internally with a ring oscillator. A diode chain circuit is used to tune the output voltage of the charge pump and create a linear negative temperature profile using a set of stacked diodes. The schematic of the diode chain circuit is shown in Fig. 11b. The exact temperature slope for the tuning voltage generator can be adjusted with the control voltage of the MOS transistor in the diode chain circuit. A low-pass MOSFET-C filter is used at the output of the charge pump to attenuate any clock ripple from modulating the resonator. The IC was fabricated in a standard  $0.5\mu\text{m}$  CMOS process and is shown in Fig. 12 with the functional blocks highlighted.

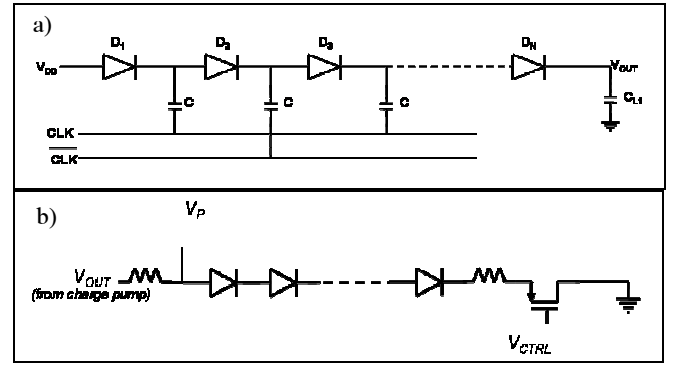


Figure 11: a) Charge pump circuit, and b) Tuning circuit for the bias generator

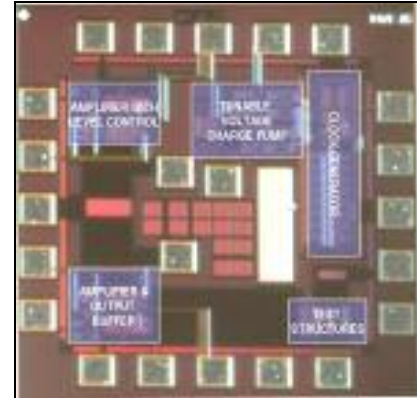


Figure 12: Die picture of the interface IC

A 4.08MHz  $I^2$  resonator (see Table 1) was interfaced with the IC to verify functionality of the oscillator. The frequency spectrum of the oscillator is shown in Fig. 13.

The temperature coefficient of frequency (TCF) of the resonator was measured in a 6-probe Desert Cryogenics vacuum probe system to be  $-26.7\text{ppm/K}$  (Fig.13). Over a  $90^\circ\text{C}$  range, the temperature drift is 2423ppm. To compensate for this drift, the generated bias voltage range, originally designed for 16-22V with a 5V supply, was scaled to 19.2-26.4V using a 6V supply. Since the ETC is  $-7.5\text{ppm/V}^2$ , this corresponds to a tuning range of 2460ppm.

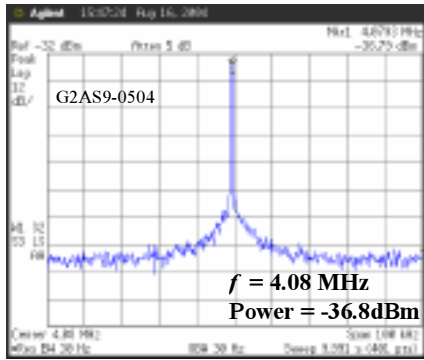


Figure 13: Frequency spectrum of an interfaced oscillator with  $V_p=10V$  at  $25^\circ C$ .

Using this temperature compensation scheme, an ideal overall frequency variation of 130ppm over the  $90^\circ C$  range is expected (Fig. 14). This variation is limited by the linear nature of the bias generator. Preliminary measurements show approximately 240ppm variation over this range, however. This discrepancy was caused by inaccuracies in the measurement setup. Nevertheless, the compensated temperature drift was reduced to 10% of the uncompensated 2400ppm.

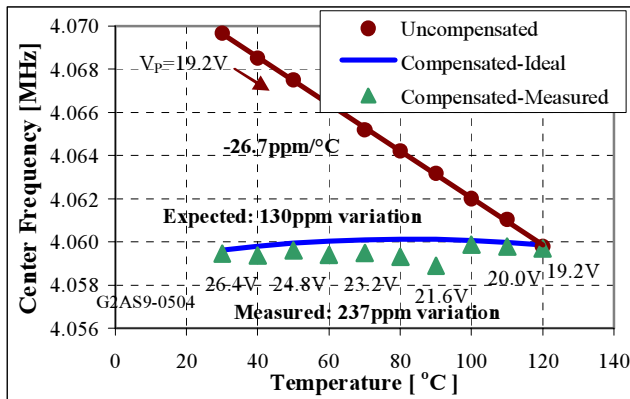


Figure 14: Uncompensated and linearly-compensated frequency-temperature drift for a 4MHz resonator over a  $90^\circ C$  range.

The accuracy of the compensation can be improved by replacing the linear bias voltage generator with one having a parabolic temperature-dependence

$$V_p^2 = A + BT \quad (7)$$

where  $A$  and  $B$  are constants. This can result in temperature variation in the order of 50ppm, thus making the temperature stability comparable to quartz oscillators.

The overall power consumption of the IC was 1.8mW (1.1mW for the amplifier and buffer and 0.7mW for the clock generator for the charge pump) and consumes an active area of 1.2mm x 0.6mm. The power consumption was largely a result of the conservative design of the ring oscillator and the buffer, both of which were designed to drive large capacitive loads.

## 5. CONCLUSIONS

A 4MHz low power consumption two-chip oscillator based on a high  $Q$ , low motional impedance, highly tunable capacitive micromechanical resonator was demonstrated. The electrode and resonator body resistances limited the optimization of the resonator admittance and loaded the resonator  $Q$ . Future implementations must resolve these loading issues. Although the electrostatic tuning coefficient was observed to decrease significantly in higher frequency resonators, this can be compensated by the use of smaller gaps. Although the temperature stability of this oscillator was greatly improved over an uncompensated device, further improvements in the compensation scheme are necessary to compete with stability of quartz-based reference oscillators. The power handling and phase noise performance will also be investigated in the near future.

## ACKNOWLEDGEMENTS

The authors thank the Georgia Tech Microelectronics Research Center cleanroom staff for their assistance. This work was funded under the DARPA NMAPS program.

## REFERENCES

- [1] Y. Ueno and H. Shimizu, "Voltage controlled temperature compensated crystal oscillator using 2-port crystal resonator," *Proc. of Intl. Frequency Control Symposium*, pp. 418-425, 1991.
- [2] Y.-W. Lin, S. Lee, S.-S. Li, Y. Xie, Z. Ren, and C. T.-C. Nguyen, "60-MHz wine-glass micromechanical-disk reference oscillator," in *Proc. ISSCC 2004*, pp. 322-323.
- [3] V. Kaajakari, T. Mattila, A. Oja, J. Kiihamäki, and H. Seppä, "Square-extensional mode single-crystal silicon micromechanical resonator for low-phase-noise oscillator applications," in *IEEE Electron Device Letters*, V25 N4, Apr2004, pp. 173-175.
- [4] S. Lee, M.U. DeMirci and C. Nguyen, "A 10-MHz micromechanical resonator Pierce reference oscillator," *Tech. Dig. Transducers 01*, pp.1094-1098., 2001.
- [5] S. Pourkamali, Z. Hao, and F. Ayazi, "VHF Single Crystal Silicon Capacitive Elliptic Bulk-Mode Disk Resonators," to be published in *JMEMS*, V13 N6, 2004.
- [6] S. Pourkamali, G. K. Ho, F. Ayazi, "Vertical Capacitive SiBARs," to be published in *Proc. IEEE MEMS'05*.
- [7] S. Pourkamali, and F. Ayazi, "Fully single crystal silicon resonators with deep-submicron dry-etched transducer gaps", in *Proc. IEEE MEMS '04*, The Netherlands, Jan. 2004, pp 813-816.
- [8] J. Dickson, "On-chip High-Voltage Generation in NMOS Integrated Circuits Using an Improved Voltage Multiplier Technique," *IEEE J. Solid-State Circuits*, vol. 11, no. 6, pp. 374-378, June 1976.